bending constants: the in-plane constant H_2 and the out-of-plane constant H_3. We have proceeded in a similar fashion with SO_4F^-. In addition, we have introduced three interaction constants to improve the agreement between the calculated and observed frequencies. The calculated frequencies are included in Tables I and III, and the corresponding valence force constants are listed in Table IV. Also included in Table III are the computed potential energy distributions for SO_4F^-. These indicate the relative contributions of the various force constants to the potential energy of each of the fundamental vibrations. (Separate potential energy distributions for ClO_4F are not given in Table I, since the dynamics of the two isoelectronic molecules are essentially the same.)

Normal-mode descriptions given in Table I for ClO_4F are equally applicable to SO_4F^-. The descriptions of the deformation modes are given in reference to ClO_3F and SO_3F^-. These descriptions are only approximate for the less symmetrical species ClO_4F and SO_4F^-. Thus the ν_5, ν_6, and ν_{10} modes of ClO_4F bear some resemblance to both the symmetrical (A_1) and the asymmetrical (E) deformation modes of ClO_3F. We have assigned ν_5 to the symmetrical deformation, because its normal motions appear to be more symmetrical than those of ν_6.

From the X-ray data we know that the SO_4F^- ion has a perchloric acid like structure, while the 1:1 correspondence that we find in the vibrational assignments of ClO_4F and SO_4F^- is consistent with a close structural resemblance between these two isoelectronic species. The valence force constants governing the motions of the ClO_3 and SO_3 moieties are essentially the same, as can be seen from Table IV, but notable differences are evident between the force constants for the O—F stretch and the O=X—O—F torsion in the two molecules. The observed frequencies are 888 and 100 cm^{-1} for ClO_4F and 830 and 150 cm^{-1} for SO_4F^-, and the two vibrations are fairly pure valence modes. We may attribute the differences to the negative charge on the fluoroxysulfate ion, which will tend to increase the electron densities on the ligand atoms. Such increased electron density in the O—F bond would be expected to lower the O—F force constant and increase the repulsion between the O—F and S=O bonds. The latter would be reflected in a stronger O=S—O—F torsion constant. Fluorine NMR data do, in fact, indicate an electron density around the fluorine in SO_4F^- greater than around that in ClO_4F.[3a,b]

It is very interesting to observe that in both SO_4F^- and ClO_4F the XO_3 rocking modes ν_{11} and ν_7 are nearly degenerate. In a pure valence force field model, we would expect the asymmetry introduced by the O—F group to split the ν_{11} and ν_7 bands by 50–100 cm^{-1}. To account for the near degeneracy in our normal-mode calculations, which assume harmonic force fields, we were forced to introduce two different O=X—O bending constants, H_2 and H_3 (see Table IV). A truer picture is probably that the low-frequency modes of X—O—F bending, ν_8, and O=X—O—F torsion, ν_{12}, are strongly coupled to the XO_3 rocking modes.

Acknowledgment. We wish to thank Dr. Karl Christe for helpful discussions of the spectral assignments and for making available to us his spectroscopic data on ClO_4F prior to publication.

Registry No. $CsSO_4F$, 70806-67-6; $RbSO_4F$, 70631-32-2; ClO_4F, 10049-03-3.

Contribution from the Chemical Crystallography Laboratory, Oxford University, Oxford, OX1 3PD, England, the Department of Chemistry, University of Missouri—Rolla, Rolla, Missouri 65401, and the Nuclear Physics Division, Atomic Energy Research Establishment, Harwell, Didcot OX11 ORA, England

A Neutron Diffraction, Magnetic Susceptibility, and Mössbauer-Effect Study of the $(Mn_xFe_{1-x})_yO$ Solid Solutions

DAVID A. O. HOPE, ANTHONY K. CHEETHAM,* and GARY J. LONG*

Received August 24, 1981

A total of 14 mixed-metal oxides, $(Mn_xFe_{1-x})_yO$, with x ranging from zero to 0.975 and y ranging from 0.910 to 0.998, have been prepared. Chemical analysis and powder neutron diffraction studies confirm that nonstoichiometry in these oxides is accommodated by the formation of defect clusters similar to those observed in Fe_yO. Magnetic susceptibility measurements from 50 to 300 K indicate that the Néel temperature decreases approximately linearly from ca. 200 K for Fe_yO to 142 K for $(Mn_{0.66}Fe_{0.34})_{0.954}O$. The room-temperature Mössbauer-effect spectra show the expected amount of high-spin iron(III) with isomer shifts in the range of 0.45 to 0.24 mm/s, decreasing with increasing manganese content. The high-spin iron(II) absorption in Fe_yO may be fitted with two quadrupole doublets with isomer shifts of ca. 1.00 and 0.95 mm/s and quadrupole interactions of ca. 0.42 and 0.80 mm/s respectively. The major new feature apparent upon the addition of manganese is a third quadrupole doublet with an isomer shift of ca. 1.05 mm/s and splittings in the range of 0.96 to 1.38 mm/s. The area-weighted average quadrupole interaction, which is ca. 0.6 mm/s for Fe_yO, increases slowly with increasing manganese content to a maximum of ca. 0.7 mm/s at 50% manganese. At higher levels of manganese, the area-weighted average quadrupole interaction drops sharply to a value of ca. 0.1 mm/s at 97.5% manganese. This behavior may be understood in terms of the number of defects present and the nature and distribution of the iron/manganese near-neighbor ions. The iron(II) isomer shift increases slightly from 0.95 to 1.10 mm/s with increasing manganese content.

Introduction

The monoxides of manganese and iron crystallize in the NaCl structure and accommodate nonstoichiometry by the oxidation of metal ions and the creation of cation vacancies. This is particularly marked in iron(II) oxide, which exists between the compositions $Fe_{0.95}O$ and $Fe_{0.88}O$ at 1000 °C and disproportionates below 570 °C.[1] The problem of the arrangement of defects in the equilibrium and quenched phases of this oxide has received a great deal of attention, and recent experimental[2-5] and theoretical[6] work suggests that the pre-

* To whom correspondence should be addressed: A.K.C., Oxford University; G.J.L., University of Missouri—Rolla.

(1) Fender, B. E. F.; Riley, F. D. *J. Phys. Chem. Solids* **1969**, *30*, 793.
(2) Andersson, B.; Sletnes, J. O. *Acta Crystallogr., Sect. A* **1977**, *A33*, 268.
(3) Greenwood, N. N.; Howe, A. T. *J. Chem. Soc., Dalton Trans.* **1972**, 110.
(4) Battle, P. D.; Cheetham, A. K. *J. Phys. C* **1979**, *12*, 337.

0020-1669/82/1321-2804$01.25/0

Table I. Summary of Neutron Diffraction and Magnetic Susceptibility Results for $(Mn_xFe_{1-x})_yO$

compd	T_d site occupancy	V^a	overall B factor, Å^2	R_{pr},[b] %	R_{nuc},[b] %	T_N, K	instrument	wavelength, Å
$(Mn_{0.05}Fe_{0.95})_{0.936}O$	0.027 (4)	3.5 (4)	0.52 (4)	6.97	2.64		DIA	1.5
$(Mn_{0.05}Fe_{0.95})_{0.954}O$	0.025 (3)	2.7 (4)	0.62 (3)	9.84	4.22		Curran	1.4
$(Mn_{0.10}Fe_{0.90})_{0.931}O$	0.034 (7)	3.0 (7)	0.78 (5)	9.66	3.69	186	Panda	1.5
$(Mn_{0.12}Fe_{0.88})_{0.926}O$	0.036 (4)	3.1 (4)	0.85 (3)	7.25	2.85		DIA	1.5
$(Mn_{0.23}Fe_{0.77})_{0.929}O$	0.031 (5)	3.3 (5)	0.71 (4)	6.69	2.76	178	Panda	1.5
$(Mn_{0.36}Fe_{0.64})_{0.954}O$	0.027 (4)	2.7 (4)	0.90 (3)	9.07	3.91	161	DIA	1.5
$(Mn_{0.50}Fe_{0.50})_{0.971}O$						158		
$(Mn_{0.56}Fe_{0.44})_{0.993}O$			0.59 (2)	4.89	2.55		DIA	1.5
$(Mn_{0.66}Fe_{0.34})_{0.954}O$	0.023 (6)	3.0 (8)	1.25 (10)	19.59[c]	13.94[c]	141[d]	DIA	1.9
$(Mn_{0.89}Fe_{0.11})_{0.997}O$			0.51 (6)	10.53	4.41		Panda	1.5

[a] The octahedral vacancy to tetrahedral interstitial ratio. [b] See ref 20 for the definition of R_{pr} and R_{nuc}. [c] Refinement of this data without the constraint (see text) gave R_{pr} = 15.1% and R_{nuc} = 7.1%. [d] A value of 158 K was obtained from neutron diffraction measurement.

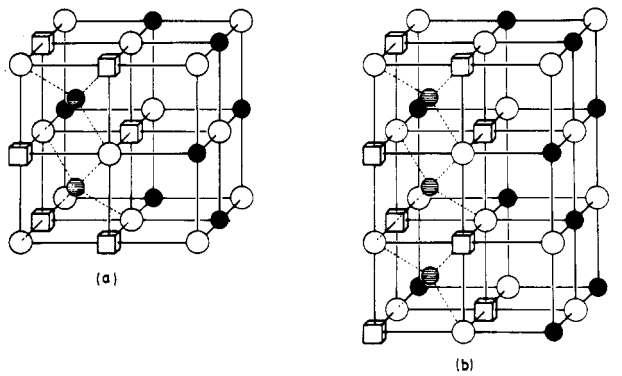

Figure 1. Defect clusters in Fe_yO: in (a), two 4:1 clusters share a common edge, and in (b), three 4:1 clusters share common edges. (a) and (b) represent 6:2 and 8:3 clusters, respectively. Filled circles are octahedral iron atoms, shaded circles are tetrahedral iron interstitials, open circles are oxygen atoms, and cubes are octahedral vacancies.

dominant defects are formed by the edge-sharing of clusters containing four iron vacancies and one tetrahedral interstitial (Figure 1). The defect structure of manganese(II) oxide is less well characterized, although defect clustering has been shown to occur.[7,8] Calculations[9] indicate that the basic unit is again the 4:1 cluster, but these aggregate by corner- rather than edge-sharing.

Among the experimental techniques capable of providing complementary information on the state of the iron(II) oxide structure are neutron diffraction and Mössbauer-effect spectroscopy. The ratio of the number of cation vacancies to tetrahedral interstitials per unit cell, and hence the average defect cluster size, can be determined by using neutron diffraction, although the technique is limited by a lack of sensitivity to the small occupancy of the tetrahedral interstitial site. Thus Battle and Cheetham,[4] in a study of quenched samples of $Fe_{0.943}O$, $Fe_{0.938}O$, and $Fe_{0.929}O$, find vacancy:interstitial ratios of 2.78, 2.82, and 3.01, respectively, suggesting the presence of 8:3 and 6:2 clusters with ratios of 2.67 and 3.0, respectively (Figure 1). These results are consistent with a similar examination of the equilibrium region.[5]

In principle, the Mössbauer effect can reveal the range of valence states and site symmetries present, but the interpretation is complicated by the complex spectra obtained. Although it has been suggested[10] that the observed resonances result from fast iron(II)–iron(III) electron exchange, most workers attribute the spectra of Fe_yO to up to two quadrupole split iron(II) doublets and a broad iron(III) singlet,[3,11,12] assignments supported by the observed spectrum of near-stoichiometric iron(II) oxide prepared under high pressure.[13]

Of the mixed crystals formed by Fe_yO, only those with MgO, CoO, and MnO show complete miscibility, a result of compatible redox behavior and ionic sizes, as discussed by Gleitzer.[14] It is only possible to attain the ideal monoxide stoichiometry in these solid solutions if the dopant cation is in very large excess. Their defect structures have not been studied in detail except for the reported similarity between the Mössbauer-effect spectra of (Fe,Mg)O and Fe_yO.[11] In (Fe,Mn)O, the room-temperature lattice constant shows an approximately linear dependence upon composition[15] and the magnetic susceptibility measurements[16] show that the Néel temperature decreases with increasing manganese content. The Néel temperature also increases with increasing iron(III) content as in iron(II) oxide.[17,18] So that variation of the paramagnetic Curie–Weiss temperature with composition could be accounted for, an ordered arrangement of iron and manganese ions has been postulated for samples containing more than 20% manganese.[16]

Experimental Section

Nine samples of $(Mn_xFe_{1-x})_yO$ were prepared by firing pellets containing the appropriate quantites of MnO, Fe_2O_3, and iron in evacuated silica tubes at 1000 °C for 24 h. The samples were quenched in liquid nitrogen. Grinding and refiring was repeated until powder X-ray diffraction and analytical electron microscopy indicated good homogeneity of the crystallites. The compositions of the samples are indicated in Tables I, II,[22] and III. The iron(II) oxide compositions were determined by gravimetric oxidation to Fe_2O_3, and the excess oxygen in the remaining samples was determined by permanganate titration for total iron and iron(II). The iron-57 specimens were prepared in quantities too small to be analyzed in this way, but their green colors indicated a negligible amount of oxidation. Their stoichiometries are calculated from the relative amounts of iron(II) and iron(III) observed in their Mössbauer spectra by using the assumption that all oxidation results in the formation of iron(III) rather than manganese(III). Analysis for the iron:manganese ratio in the solid solutions was carried out by atomic absorption and verified in the analytical electron microscope by measuring the relative intensities of the X-ray Kα emission lines. The details of the agreement obtained have been discussed by Cheetham and Skarnulis.[19] In addition, the

(5) Gavarri, J. R.; Carel, C.; Weigel, D. *J. Solid State Chem.* **1979**, *29*, 81.
(6) Catlow, C. R. A.; Fender, B. E. F. *J. Phys. C* **1975**, *8*, 3267.
(7) Hed, A. Z.; Tannhauser, D. S. *J. Electrochem. Soc.* **1976**, *114*, 314.
(8) Leroy, B.; Leroy, Y.; Lacombe, P. *J. Phys. Chem. Solids* **1972**, *33*, 1515.
(9) Catlow, C. R. A.; Fender, B. E. F.; Muxworthy, D. G. *J. Phys. (Paris), Colloq.* **1977**, *12*, 67.
(10) Elias, D. J.; Linnett, J. W. *Trans. Faraday Soc.* **1969**, *65*, 2673.
(11) Johnson, D. P. *Solid State Commun.* **1969**, *7*, 1785.
(12) Shirane, G.; Cox, D. E.; Ruby, S. L. *Phys. Rev.* **1962**, *125*, 1158.
(13) Simons, B.; Siefert, F. *Year Book—Carnegie Inst. Washington* **1978**, 625.
(14) Gleitzer, C. *Mater. Res. Bull.* **1980**, *15*, 507.
(15) Foster, P. K.; Welch, A. J. E. *Trans. Faraday Soc.* **1956**, *52*, 1626.
(16) Evrard, O. *Rev. Chim. Mineral.* **1971**, *8*, 63.
(17) Koch, F.; Fine, M. E. *J. Appl. Phys.* **1966**, *38*, 1470.
(18) Mainard, R.; Boubel, M.; Fousse, H. *C. R. Hebd. Seances Acad. Sci.* **1968**, *266*, 1299.
(19) Cheetham, A. K.; Skarnulis, A. J. *Anal. Chem.* **1981**, *53*, 1060.

Table III. Mössbauer-Effect Spectral Data[a]

	iron(III)				iron(II)													
					inner doublet				central doublet				outer doublet				total	
compd	δ	Γ	%A^b	%A^c	δ	ΔE_Q	Γ	%A	δ	ΔE_Q	Γ	%A	δ	ΔE_Q	Γ	%A	area[d]	χ^2
$Fe_{0.910}O$	0.43	0.64	19.7	9.0	0.99	0.42	0.39	31.1	0.95	0.80	0.48	59.9					37.1	4.37
$Fe_{0.918}O$	0.42	0.51	17.9	7.5	1.00	0.43	0.37	38.7	0.94	0.80	0.43	53.8					36.5	2.22
$(Mn_{0.10}Fe_{0.90})_{0.931}O$	0.35	0.71	16.3	12.3	1.03	0.40	0.37	26.9	1.00	0.74	0.36	35.8	1.00	1.14	0.36	21.0	29.8	2.44
$(Mn_{0.23}Fe_{0.77})_{0.929}O$	0.25	0.69	19.7	15.8	1.03	0.53	0.41	36.3	1.02	0.92	0.36	29.0	1.04	1.34	0.35	15.0	25.8	1.64
$(Mn_{0.36}Fe_{0.64})_{0.954}O$	0.22	0.56	15.0	13.5	1.05	0.54	0.39	44.6	1.04	0.89	0.33	22.4	1.06	1.29	0.42	19.5	21.2	1.57
$(Mn_{0.50}Fe_{0.50})_{0.971}O$	0.19	0.64	11.8	11.8	1.06	0.52	0.37	51.3	1.06	0.89	0.37	25.7	1.05	1.34	0.41	11.2	16.4	1.68
$(Mn_{0.56}Fe_{0.44})_{0.993}O$	0.20	0.42	3.1	4.2	1.06	0.44	0.34	52.6	1.06	0.73	0.33	31.1	1.05	1.12	0.48	13.2	16.2	1.09
$(Mn_{0.66}Fe_{0.34})_{0.954}O$	0.24	0.68	28.3	28.6	0.97	0.43	0.41	11.7	1.08	0.50	0.32	25.7	1.10	0.96	0.54	34.3	15.0	1.36
$(Mn_{0.90}{}^{57}Fe_{0.10})_{0.997}O$	0.24	0.76		5.2	1.08	0.34	0.42	94.8										1.10
$(Mn_{0.975}{}^{57}Fe_{0.025})_{0.998}O$	0.03	1.2		15.1	1.08		0.42	43.7	1.06	0.28	0.39	41.2						1.05

[a] All data obtained at room temperature and given in mm/s relative to natural α-iron foil. [b] The percentage of total iron as iron(III) as determined from analytical data and constrained in the spectral fits. [c] The percentage of total iron as determined from unconstrained Mössbauer spectral fits. [d] In units of % mm/s for a constant absorber thickness.

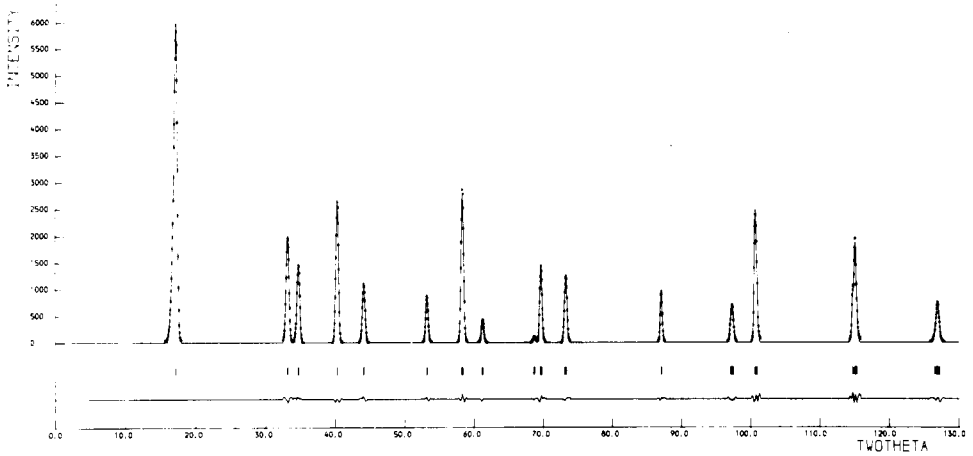

Figure 2. Observed (points) and calculated (line) powder neutron diffraction profile obtained at 5 K for $(Mn_{0.56}Fe_{0.44})_{0.993}O$. A difference curve is also shown below the profile. The data include both magnetic and nuclear reflections.

spread of values obtained from electron microscopy measurements on 10 different crystallites of each solid solution was used to gauge sample homogeneity, and, if necessary, further firings were carried out.

Neutron powder diffraction profiles were recorded at 4.2 K on the diffractometers D1A at the ILL, Grenoble, France, and Panada and Curran at AERE, Harwell, England. The samples were placed in 12-mm diameter vanadium cans located in cryostats with vanadium or aluminum tails, and data were collected in the 2θ range of ca. 6–120°. All specimens are magnetically ordered at 4.2 K, but the magnetic periodicity is such that the magnetic and nuclear reflections are separate, as shown in Figure 2. A data set was normally recorded in 24 h, although on the lower flux AERE diffractometers this time was sometimes extended. In the line-profile analysis[20] of the nuclear scattering, the rhombohedral space group $R\bar{3}$ was used with octahedral metal ions on the 1*a*, tetrahedral metal ions on the 2*c* (with *x* fixed at 0.25), and oxygen ions on the 1*b* sites. The occupancy numbers of the octahedral and tetrahedral sites were constrained according to the results of the chemical analysis: all the available manganese was assumed to occupy the octahedral site, and the occupancies of the octahedral and tetrahedral sites by iron were constrained to equal the analytically determined iron content. This procedure was not adopted with the samples showing small deviations from stoichiometry, $(Mn_{0.56}Fe_{0.44})_{0.993}O$ and $(Mn_{0.89}Fe_{0.11})_{0.997}O$, where the tetrahedral occupancy was negligible; here the constraint was applied simply to the iron and manganese content of the octahedral site. In addition, refinements of the $(Mn_{0.66}Fe_{0.34})_{0.954}O$ data were substantially improved by removing the occupancy number constraint, as indicated in Table I. The octahedral vacancy to tetrahedral interstitial ratios obtained and the final line profile and nuclear intensity reliability indices are presented in Table I.

(20) Rietveld, H. M. *J. App. Crystallogr.* **1969**, *2*, 65.

Mössbauer-effect absorbers were prepared by mixing fine powders with Vaseline and contained 50 mg of sample/cm^2. The spectra were obtained on either a Range Electronics or a Harwell constant-acceleration spectrometer, both of which used a room-temperature rhodium-matrix source and were calibrated at room temperature with natural α-iron foil. Least-squares minimization programs implemented on the IBM 370/168 at Harwell and the Amdahl 7 at the University of Missouri—Rolla were used to analyze the spectra, and the parameters reported have errors of approximately 0.02 mm/s. The spectra are modeled with a single broad high-spin iron(III) resonance and up to three high-spin iron(II) quadrupole doublets. The components of the quadrupole doublets are constrained to be equal in width and area.

Magnetic susceptibility measurements between 50 and 300 K were obtained on a Faraday balance with a Janis Supervaritemp cryostat and a Lake Shore Cryotronics temperature controller.[21] Temperatures were measured with a calibrated silicon diode and are accurate to approximately 0.1% of the absolute temperature. The magnetic field was measured with a Hall probe, and the balance was calibrated with $CoHg(NCS)_4$. The resulting Néel temperatures are given in Table I and are plotted for comparison with earlier work in Figure 3.[22] Figure 4 shows the overall variation of the magnetic susceptibility with temperature for each composition studied. It is not possible to obtain values for the paramagnetic Curie temperatures because the data do not extend to sufficiently high temperatues.

Results and Discussion

The difference in neutron-scattering lengths between manganese (-0.37×10^{-14} m) and iron (0.95×10^{-14} m) makes

(21) Long, G. J.; Longworth, G.; Battle, P.; Cheetham, A. K.; Thundathil, R. V.; Beveridge, D. *Inorg. Chem.* **1979**, *18*, 624.
(22) Supplementary material.

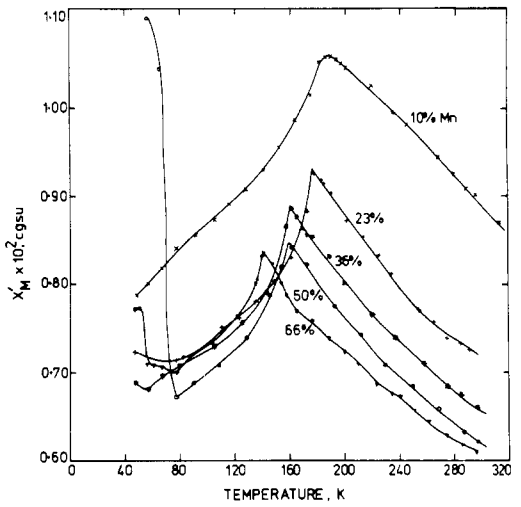

Figure 4. Magnetic susceptibility as a function of temperature for several compositions.

neutron diffraction a good method for the detection of any long-range atomic ordering of iron and manganese such as that suggested by Evrard.[16] No nuclear superlattice reflections are observed at 4.2 K in any of the neutron profiles, but that of $(Mn_{0.66}Fe_{0.34})_{0.954}O$ shows an appreciable amount of diffuse scattering around both nuclear and magnetic peaks. This scattering is independent of temperature and appears to be due to a lack of gross homogeneity although different electron microscopic analyses agree well, the powder X-ray diffraction lines are sharp, and the Néel temperature is well-defined (Figure 4). The vacancy:interstitial ratios (Table I) range from 2.7 to 3.6 and are in agreement with those deduced in similar studies of pure iron(II) oxide.[4] However, the more precise values obtained from the D1A diffractometer, with its higher flux and flatter background, are grouped closely together in the range 2.7–3.1 and strongly suggest the presence of 6:2 and 8:3 clusters.

The Néel temperatures, as determined by magnetic susceptibility measurements in the present and in earlier studies,[16] are plotted in Figure 4. Numerical data are given in Table II.[22] A gradual decrease of T_N with increasing manganese content and an increase with departure from monoxide stoichiometry is confirmed. The ordering temperature of $(Mn_{0.66}Fe_{0.34})_{0.954}O$ has also been measured independently by neutron diffraction and, surprisingly, is found to be somewhat higher (see Table I). However, this difference may stem largely from the difficulty inherent in estimating the intensity of a weak magnetic reflection in the presence of the substantial diffuse scattering observed with this sample.

Another feature of the magnetic data is the increase in susceptibility at temperatures below 60 K for samples containing 23% or more manganese. Although not detected by diffraction methods, this can be attributed to trace amounts of ferrimagnetic Mn_3O_4, which has an ordering temperature of 43 K and has been shown to dominate the low-temperature magnetic behavior of MnO.[23] It does not follow from the observation that the impurity is pure Mn_3O_4 because Fe_3O_4 and Mn_3O_4 show appreciable mutual solubility.[24] It is possible that the impurity is a manganese-rich $(Mn_xFe_{1-x})_3O_4$ that orders below 60 K.[25]

The Mössbauer-effect spectra obtained at room temperature are illustrated in Figures 5 and 6, and the resulting parameters are presented in Table III. Marked changes are apparent in the spectra as the proportion of manganese increases. For the purpose of fitting these spectra, it has been assumed that all the iron(II) and iron(III) is present in the high-spin state and

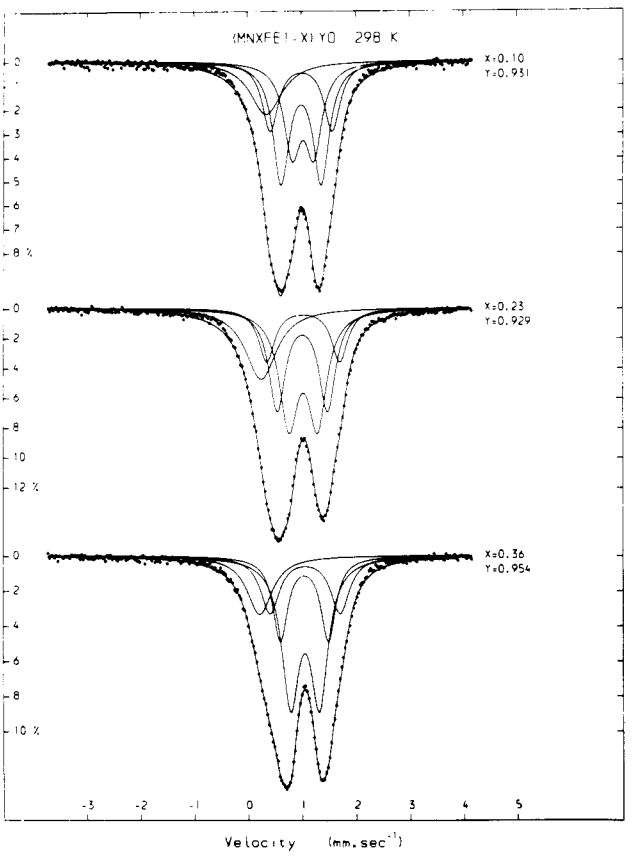

Figure 5. Room-temperature Mössbauer-effect spectra of $(Mn_xFe_{1-x})_yO$.

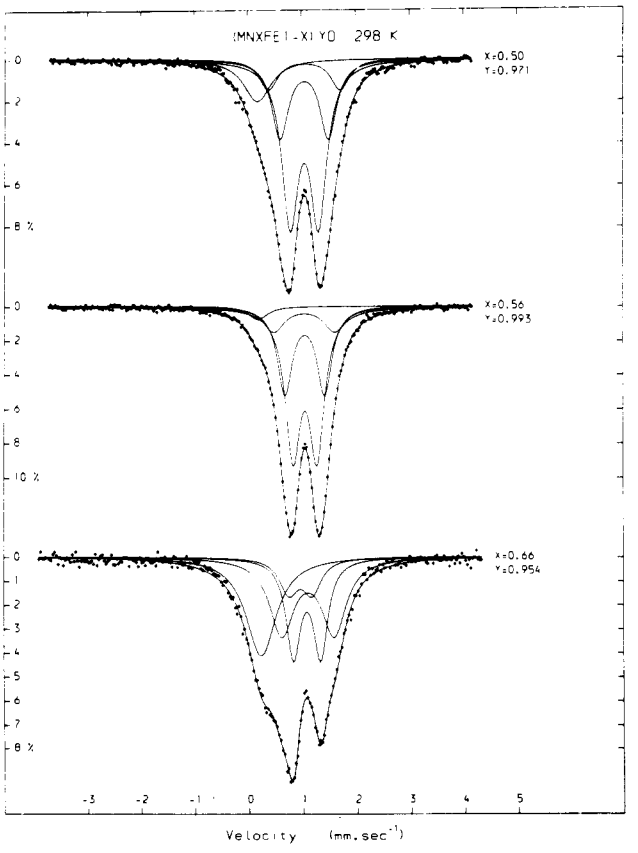

Figure 6. Room-temperature Mössbauer-effect spectra of $(Mn_xFe_{1-x})_yO$.

(23) Jagadeesh, M. S.; Seehra, M. A. *Phys. Rev. 1980, B21*, 2897.
(24) Van Hook, H. J.; Keith, M. L. *Am. Mineral.* **1958**, *43*, 80.
(25) Yun, I. *Mem. Fac. Sci., Kyoto Univ., Ser. Geol. Mineral.* **1958**, *25*, 125.

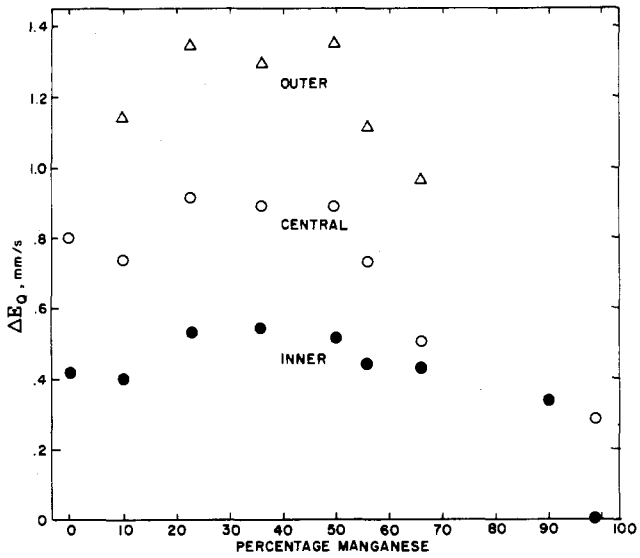

Figure 7. Composition dependence of the inner, central, and outer iron(II) quadrupole doublets in $(Mn_xFe_{1-x})_yO$.

that contributions to the iron(II) quadrupole interaction arise from the proximity of cation vacancies, iron(III) ions, and asymmetric, near-neighbor iron/manganese distributions. Despite the large number of factors contributing to the quadrupole interaction and isomer shift, some trends can be distinguished.

The iron oxide spectra are well represented by an iron(III) singlet and two iron(II) quadrupole doublets as has been reported previously,[3,11] although it is noteworthy that the proportion of iron(III) is much less than that determined by chemical analysis (Table II). The solid-solution spectra could not be fitted with the five-line model and required the inclusion of a third quadrupole doublet with a splitting in the range of 0.90–1.38 mm/s, a component not found in the Fe_yO spectra. The need for this additional component is clearly demonstrated in Figures 5 and 6. The composition dependence of the quadrupole splittings found for these three doublets is shown in Figure 7, which demonstrates the combined effect of the lowering of the iron(II) site symmetry by the proximity of manganese and the large number of vacancies and iron(III) ions present at low-manganese contents. Because of the broad unresolved nature of the various iron(II) quadrupole doublet components in these spectra, it is difficult to make specific assignments of any set of lines to a specific structural feature. However, because we have obtained spectra for a range of compositions, it is possible to draw some general conclusion about the different components as a function of manganese, vacancy, and interstitial content. We choose to do this in terms of the area-weighted average quadrupole splitting because this is a parameter which is basically independent of the specific model used to fit the spectra. The influence of the manganese upon the asymmetry of the iron(II) site is most easily seen in the plot of the area-weighted average quadrupole splitting shown in Figure 8. For the two iron(II) oxide spectra, the averaged quadrupole interactions are 0.597 and 0.610 mm/s, with decreasing iron content. The average value of 0.60 mm/s, shown in Figure 8, underlines the importance of the defects in determining the average quadrupole interaction in Fe_yO; the corresponding value for "FeO" prepared under high pressure[13] (which presumably has a very low defect concentration) is approximately 0.21 mm/s. The lack of variation of the averaged quadrupole splittings as a function of composition in the Fe_yO samples presumably stems from the high concentration of defects present; essentially all the iron(II) ions are subject to their influence. As the manganese content increases to a value of ca. 50%, the averaged quadrupole interaction increases slowly to a value of between 0.65 and 0.70 mm/s. This increase no doubt arises because of the presence of both manganese and iron near neighbors, producing an enhanced electric field gradient at the iron (II) sites and it is reflected in the additional, outer quadrupole doublet that is now required to fit the spectra (see Figures 5 and 6 and Table III).

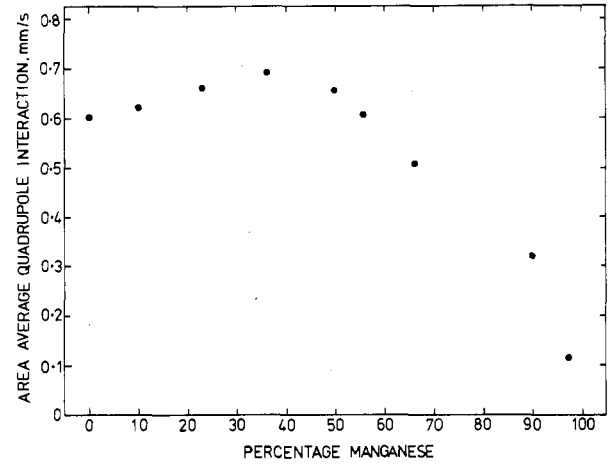

Figure 8. Composition dependence of the area-weighted average iron(II) quadrupole interaction in $(Mn_xFe_{1-x})_yO$.

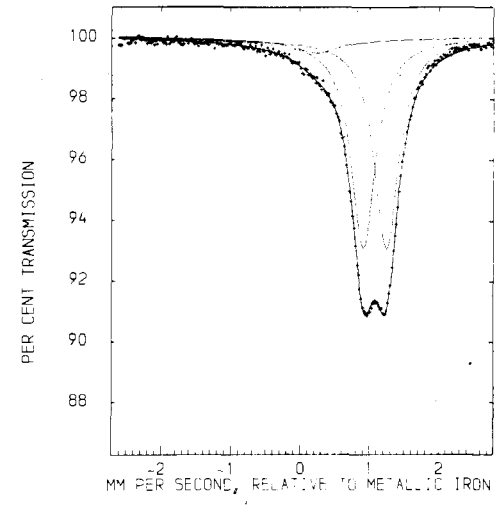

Figure 9. Room-temperature Mössbauer-effect spectrum of $(Mn_{0.90}{}^{57}Fe_{0.10})_{0.997}O$.

Table IV. Fraction of Iron Sites with i Manganese Near-Neighbor Atoms

i	$(Mn_{0.975}{}^{57}Fe_{0.025})_{0.998}O$	$(Mn_{0.90}{}^{57}Fe_{0.10})_{0.997}O$
12	0.739	0.282
11	0.225	0.377
10	0.033	0.230
9	0.003	0.085
8	0	0.021
7	0	0.004

At higher levels of manganese content, the area averaged quadrupole interaction falls rapidly to a value of ca. 0.1 mm/s at 97.5% manganese. The small quadrupole splitting observed in the iron-57-enriched samples, as illustrated in Figure 9, indicate that the proportion of iron(II) in a near-cubic environment increases markedly from $(Mn_{0.90}{}^{57}Fe_{0.10})_{0.997}O$ to $(Mn_{0.975}{}^{57}Fe_{0.025})_{0.998}O$. This increase results because there is both a decrease in the number of defects and an increase in the iron(II) site symmetry as a result of the predominance of manganese in the near-neighbor sites. This trend is illustrated by the binomial calculation, presented in Table IV, of

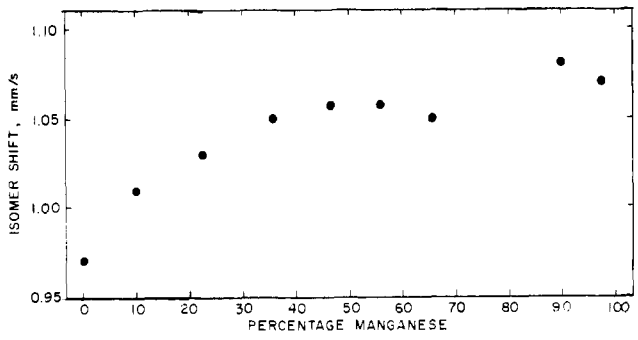

Figure 10. Composition dependence of the average iron(II) isomer shift for $(Mn_xFe_{1-x})_yO$.

the fraction of iron sites which have i manganese and $12 - i$ iron near neighbors.

It should be noted that both $(Mn_{0.66}Fe_{0.34})_{0.954}O$ and $(Mn_{0.36}Fe_{0.64})_{0.954}O$ have the same metal:oxygen ratio but very different Mössbauer-effect spectra (see Figures 5, 6, and 8). The spectrum of $(Mn_{0.66}Fe_{0.34})_{0.954}O$ closely resembles that of iron(II) oxide, indicating that the effects of the random M^{2+} cation distribution are less pronounced here. This is consistent with the large proportion of the total iron as iron(III) (ca. 30%), and a proportionately smaller amount of iron(II), that gives rise to a diminished number of these ions in low-symmetry sites. A related observation is the similarity between the spectrum of $(Mn_{0.975}{}^{57}Fe_{0.025})_{0.998}O$ and that of "FeO" [13] in which, again, more iron(II) ions are in high-symmetry sites.

The Mössbauer-effect isomer shift values, reported in Table III, although typical of divalent and trivalent iron in an oxide lattice show some unusual features as a function of composition. The isomer shift of iron(II) increases with increasing manganese content (Figure 10), which suggests that the iron(II) d electrons are becoming more localized compared with those in iron(II) oxide, leading to increased s electron screening. This is compatible with the greater electronegativity of iron(II) compared to manganese(II) and therefore suggests that iron(II)–manganese(II) charge transfer (via the cation–cation interactions) is weaker than that involving two iron(II) ions. The iron(III) isomer shift decreases markedly with increasing manganese concentration, indicating that the s electron density at the nucleus is increasing. So that the local charge neutrality can be preserved, the iron(III) ions are concentrated around defect clusters and in the solid solutions their nearest-neighbor iron(II) ions are progressively replaced by manganese(II). This again decreases the ease of charge transfer and forces the "iron(II)" ions to be more like iron(III). These observations suggest that electrons with appreciable itinerant characteristics are present in the immediate vicinity of the defect clusters in iron(II) oxide.

In our fits of the Mössbauer spectra, we have used a broad singlet for the iron(III) line rather than a quadrupole doublet. This is reasonable because the iron(III) has a $^6A_{1g}$ ground state and hence only a very small valence contribution to the electric field gradient. The broadening of the line results from a significant lattice contribution to the electric field gradient. The 4:1 cluster and its surroundings should give rise to an overall asymmetry sufficient to broaden the iron(III) band. However, in $(Mn_{0.90}{}^{57}Fe_{0.10})_{0.997}O$ and $(Mn_{0.975}{}^{57}Fe_{0.025})_{0.998}O$, the iron(III) band is much broader. This increased line width may be associated with more extensive dissociation of the 4:1 clusters into isolated vacancy:iron(III) complexes at low iron content or the presence of iron-57-substituted Mn_3O_4 as is observed in low-temperature spectra.[26]

The agreement between the volumetric iron(III) analysis and the proportion of iron(III) detected by the Mössbauer effect is very good, except for those samples showing the greatest deviations from the ideal monoxide stoichiometry. In these cases the amount of iron(III) observed in the Mössbauer spectra is less than that expected from the analytical results. Usually, one would expect the amount of iron(III) relative to iron(II) observed in the Mössbauer-effect spectrum to be high because of the higher recoil-free fraction expected for the trivalent ion, which has a higher binding energy. However, for the compounds under study, the iron(III) ions tends to be associated in clusters with vacancies and hence the opportunity for iron(III) recoil is greater than for the iron(II) sites.

Acknowledgment. It is a pleasure to acknowledge the assistance and helpful discussions with Drs. J. B. Goodenough, A. W. Hewat, C. Wilkinson, G. Longworth, T. E. Cranshaw, and P. Battle, Mrs. A. E. Stoker, and Messrs. B. Laundy, L. Becker, S. M. Tetrick, and S. Heathman. We thank the AERE University Support Group of Experimental assistance, the Science Research Council for the provision of the neutron facilities, and a research studentship for D.A.O.H., NATO for a cooperative scientific research grant, and USAF for a support grant (AFOSR-79-0120).

Registry No. MnO, 1344-43-0; FeO, 1345-25-1.

Supplementary Material Available: A listing of magnetic susceptibility data (Table II) and an illustration of the Néel temperature as a function of manganese content (Figure 3) (5 pages). Ordering information is given on any current masthead page.

(26) Hope, D. A. O.; Cheetham, A. K.; Long, G. J., in preparation.